Analysis of Relative Motion of Collocated Geostationary Satellites with Geometric Constraints

F.J. de Bruijn[1], E. Gill[2]

Abstract

This paper investigates the design of the relative motion orbits of geostationary satellites in the presence of geometric constraints. A geometric constraint is defined by a sensor's pointing direction and field of view. An analyis was made of the underlying geometry of the relative orbits associated to geometric constraints. This resulted in the derivation of novel relations between relative orbital elements and geometric constraints. The paper presents a set of guidelines that can support the design of relative orbits, that use the relations between the orbital elements and constraints. These guidelines are applied in a characteristic example that includes a nadir-pointing sensor and a north-looking star sensor. The focus in this paper is on collocated satellites in geostationary orbits. The results were derived for near-circular orbits, where the satellites share the same mean argument of longitude. The developed relations can likewise be applied for other types of collocated satellites.

Keywords: Relative Orbit Design, Collocation, Geometric Constraints, Relative Motion, Sensor Constraints

1. Introduction

Collocation of geostationary satellites is generally achieved using the so called eccentricity/inclination (e/i) vector separation [1]. This method is based on the fact that estimation, prediction and control of relative motion in radial and normal direction is generally more accurate than in tangential direction [1]. By maximizing the separation in radial direction at zero separation in normal direction, and vice versa, the risk of collisions is minimized. This same method is applied in Low Earth Orbit (LEO), for example for the TerraSAR-X/TanDEM-X formation [2] and the PRISMA mission [3]. The concept is also of high interest for clusters of fractionated spacecraft, where generally no specific formation geometry requirements are present, apart from minimum and maximum separation distances [4].

When using the concept of e/i vector separation, one satellite may enter the field of view of the sensors on one of the other satellites in the cluster, at some point in time during relative motion. For a cluster controlled using the principle of e/i vector separation this is, e.g., the case for nadir-pointing sensors (assuming that the satellites are controlled towards the same mean argument of longitude), but it may also happen for star sensors. Depending on the type of sensor that is blocked (or interfered with) this could, for example, result in an outage of the signal, an impediment of an observation, or a loss of attitude information [5]. A potential solution to this problem of sensor interference lies in the design of specific relative motion orbits which could avoid such situations.

Relative orbit design methods for formation flying [6], cluster flight [4] and collocated geostationary satellites [1] are present in the literature. However, the problem of sensor interference is not treated as part of the relative orbit design problem. The goal of this paper is, based on an analysis of a set of geometric constraints in terms of a sensor's pointing direction and field of view, to provide a set of guidelines for designing relative motion orbits for collocated geostationary satellites that respect the geometric constraints.

Email addresses: Frederik.Bruijn@DLR.de (F.J. de Bruijn), E.K.A.Gill@tudelft.nl (E. Gill)

[1]German Aerospace Center (DLR), Institute of Space Systems, Bremen, Germany,

[2]Delft University of Technology, Chair of Space Systems Engineering, Delft, The Netherlands

In Section 2, the relative orbits, parameterized in relative orbital elements, are introduced. In the same section, the geometric constraint is formally defined and the underlying geometry is analysed. Section 3 provides the results of the analysis, including a set of guidelines for relative orbit design in the presence of geometric constraints. A worked-out example with a nadir-pointing sensor and a north-looking star sensor is presented as well. The last part of the paper includes a discussion on the domain of validity of the results and real-world considerations, followed by the conclusion and outlook.

2. Theory of Geometry Constrained Relative Motion

2.1. Relative Motion

In this paper, the focus is on geostationary orbits, and therefore, absolute orbits were chosen to be defined by the equinoctial orbital elements

$$\mathbf{E} = \begin{pmatrix} a \\ \lambda \\ e_x \\ e_y \\ i_x \\ i_y \end{pmatrix} = \begin{pmatrix} a \\ \Omega + \omega + M \\ e\cos(\Omega + \omega) \\ e\sin(\Omega + \omega) \\ i\cos\Omega \\ i\sin\Omega \end{pmatrix}, \qquad (1)$$

where a, e, i, ω, Ω and M are classical Keplerian elements. Figure 1 illustrates the eccentricity vector $\mathbf{e} = (e_x, e_y)^T$, the inclination vector $\mathbf{i} = (i_x, i_y)^T$ and the mean argument of longitude λ. The relative orbital elements between two satellites are obtained by differencing their absolute orbital elements

$$\Delta\mathbf{E} = \begin{pmatrix} \Delta a \\ \Delta\lambda \\ \Delta e_x \\ \Delta e_y \\ \Delta i_x \\ \Delta i_y \end{pmatrix} = \begin{pmatrix} a_i - a \\ \lambda_i - \lambda \\ e_{x_i} - e_x \\ e_{y_i} - e_y \\ i_{x_i} - i_x \\ i_{y_i} - i_y \end{pmatrix}. \qquad (2)$$

Here, the subscript i distinguishes the other satellite(s) from the main satellite. For satellites having the same semi-major axis and the same mean argument of longitude, the relative orbits have an elliptical shape with one satellite being exactly in the center of the ellipse. In this case, the relative motion is completely characterized by the relative eccentricity and inclination vectors. These vectors can be written in polar form as [3]

$$\Delta\mathbf{e} = \begin{pmatrix} \Delta e_x \\ \Delta e_y \end{pmatrix} = \delta e \begin{pmatrix} \cos\varphi \\ \sin\varphi \end{pmatrix} \qquad (3)$$
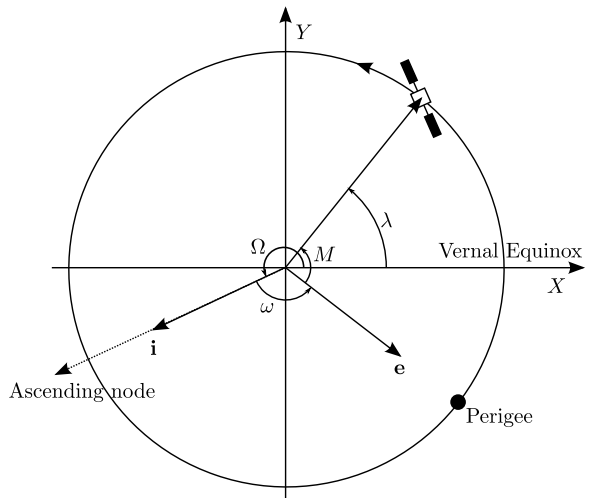

Figure 1: Eccentricity and inclination vectors in the equatorial plane.

$$\Delta\mathbf{i} = \begin{pmatrix} \Delta i_x \\ \Delta i_y \end{pmatrix} = \delta i \begin{pmatrix} \cos\theta \\ \sin\theta \end{pmatrix}, \qquad (4)$$

where $\delta e = \|\Delta\mathbf{e}\|$ and $\delta i = \|\Delta\mathbf{i}\|$ are the radial polar coordinates and ϕ and θ are the angular polar coordinates. The relative phasing angle $\psi = \varphi - \theta$ completely determines the orientation of the relative motion orbit, while $a\delta e$ and $a\delta i$ determine its size. Projected on the orbital plane, the relative motion is a 2:1 ellipse, with semi-major axis $2a\delta e$ in tangential direction and semi-minor axis $a\delta e$ in radial direction [3]. The motion in cross-track direction is independent of the motion in the orbital plane and is characterized by a sinusoidal motion with orbital period and an amplitude equal to $a\delta i$. This causes the relative motion orbits to lie on the sides of an elliptical cylinder as graphically shown in Figure 2. The point where the orbit hits the top of the cylinder (i.e., the point where the cross-track motion has its maximum) depends on the relative phasing angle ψ.

2.2. Geometric Constraints

The geometric constraints treated in this paper are simple conic sensor constraints, defined by a sensor's line of sight and a sensor's half angle, together constituting the sensor's field of view. Violation of the constraint occurs when a satellite enters the field of view of a sensor on another satellite. Figure 3 shows the involved vectors and angles graphically. The viewing direction is defined by the unit vector $\mathbf{e}_c$ and the sensor's half angle is $\beta/2$. In
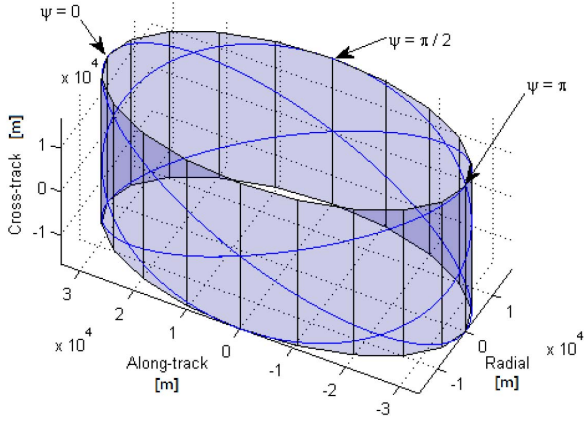
Figure 2: Relative orbits are confined to an elliptical cylinder for $\Delta a = 0$ and $\Delta \lambda = 0$

.

this paper, the viewing direction is assumed to be constant in the Hill frame (also known as the Radial, Tangential, Normal (RTN) frame or a rotated Local Vertical, Local Horizontal (LVLH) frame), corresponding to, e.g., a nadir-pointing satellite. The unit vector $\mathbf{e}_{01}$ points from satellite 0 to satellite 1 and α is the angle between $\mathbf{e}_c$ and $\mathbf{e}_{01}$, so that the constraint is defined as follows:

$$\mathrm{acos}\left(\mathbf{e}_c \cdot \mathbf{e}_{01}\left(t\right)\right) = \alpha\left(t\right) > \beta/2, \qquad (5)$$

or

$$\mathbf{e}_c \cdot \mathbf{e}_{01}\left(t\right) < \cos\left(\beta/2\right). \qquad (6)$$
$$\text{for} \quad \alpha, \beta \in [0, \pi]$$

Note that since satellite 1 moves with respect to satellite 0, α is a function of time. This constraint is referred to as a geometric constraint in the remainder of this paper.

Instead of checking satisfaction of the constraint for every point in the orbit it would suffice to check satisfaction of the constraint at the point in the orbit where α reaches its minimum $\alpha_{\min}$. Figure 4 shows the relative orbit of satellite 1 around satellite 0.

The angle between the constraint vector and its projection on the relative orbital plane is the smallest angle $\alpha_{\min}$ over a full relative orbit. This angle shall be larger than the sensor's half angle $\beta/2$, as per Figure 4. The vector $\mathbf{e}_\perp$ is the vector perpendicular to the relative orbital plane and defines the orientation of the relative orbital plane. If this vector is known, it is easy to check potential violation of the constraint:
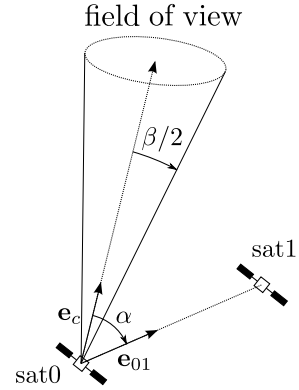

Figure 3: Graphical representation of the parameters involved in defining the geometric constraint
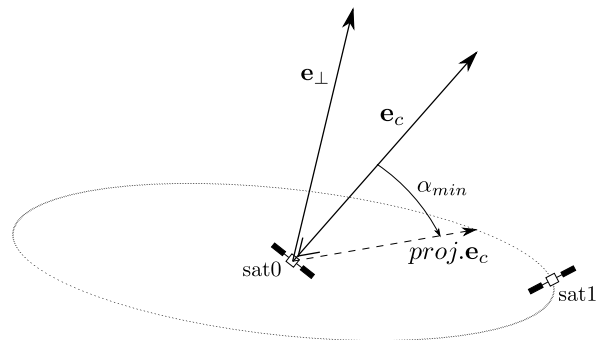

Figure 4: Visualization of $\alpha_{\min}$ and its relation to $\mathbf{e}_\perp$

3

$$\alpha_{\min} = \pi/2 - \text{acos} \left(\mathbf{e}_\perp \cdot \mathbf{e}_c \right) \qquad (7)$$

$$\alpha_{\min} > \beta/2 \quad \text{or} \quad \sin\left(\beta/2\right) < \mathbf{e}_\perp \cdot \mathbf{e}_c \qquad (8)$$

Both unit vectors $\mathbf{e}_\perp$ and $\mathbf{e}_c$ can be defined in terms of their azimuth and elevation angles, γ and χ respectively, in the Hill frame. The definition of these angles is indicated for $\mathbf{e}_c$ in Figure 5 with the following domain:

$$\begin{array}{rcl} \gamma_c & \in & [0, 2\pi) \\ \chi_c & \in & [-\pi/2, \pi/2] \\[6pt] \gamma_\perp & \in & [0, 2\pi) \\ \chi_\perp & \in & [0, \pi/2], \end{array} \qquad (9)$$

i.e., the sensor can point in any direction, while $\mathbf{e}_\perp$ is confined to the hemisphere with a positive component in Z-direction.

The unit vector perpendicular to the relative orbital plane can be derived from the relative orbital elements. To that end, a circular projection of the orbit in the (X, Y)-plane of the Hill frame is assumed by dividing the Y-component of relative motion by two (due to the natural 2:1 ellipse of the relative motion in (X, Y)-direction). The angle $\chi'_\perp$ corresponds to the direction of relative angular momentum for the orbit with the circularized (X, Y)-projection. The angle $\gamma_\perp$ remains unaltered. If ψ is the relative phasing angle between the inclination and eccentricity vector, $\gamma_\perp$ and $\chi'_\perp$ are given by

$$\chi'_\perp = \text{atan} \left(\frac{\|\Delta \mathbf{e}\|}{\|\Delta \mathbf{i}\|} \right), \quad \gamma_\perp = \psi - \frac{\pi}{2}. \qquad (10)$$

The unit vector perpendicular to the circularized relative orbit can be obtained from Eqs. 10. The unit vector of the actual 2:1 elliptical shaped relative orbit is retrieved by multiplying the Y-component by a factor $1/2$ and normalizing the result, so that

$$\mathbf{x}_\perp = \begin{pmatrix} \cos\left(\gamma_\perp\right)\cos\left(\chi'_\perp\right) \\ 0.5 \sin\left(\gamma_\perp\right)\cos\left(\chi'_\perp\right) \\ \sin\left(\chi'_\perp\right) \end{pmatrix} \qquad (11)$$

and

$$\mathbf{e}_\perp = \frac{\mathbf{x}_\perp}{\|\mathbf{x}_\perp\|}. \qquad (12)$$

For fixed δe and δi, the relative motion orbits, generated by varying ψ, trace out an elliptical cylinder as shown in Figure 6. This cylinder is symmetric with respect to X-, Y- and Z-axis. A constraint
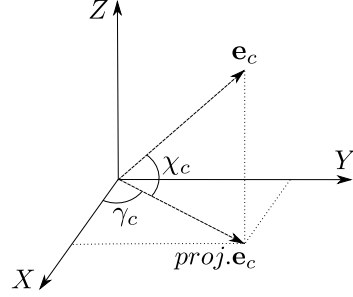

Figure 5: Orientation of $\mathbf{e}_c$ as defined by azimuth γ_c and elevation ξ_c in the Hill frame.

in an arbitrary direction may always be brought back to a constraint in the positive orthant $\mathbb{R}^3_+$, by mirroring the constraint vector over the (X, Y)- and/or (X, Z)- and/or (Y, Z)-plane. The same is true for a result of an analysis for a constraint in $\mathbb{R}^3_+$, it can be brought back to a result for a constraint in an arbitrary direction (with the relative phasing angle ψ as a result). Results for the other orthants can be derived from results in $\mathbb{R}^3_+$ using the following transformations:

1. Mirroring the constraint over the (X, Y)-plane: $\psi = \psi_{\mathbb{R}^3_+} + \pi$
2. Mirroring the constraint over the (X, Z)-plane: $\psi = -\psi_{\mathbb{R}^3_+}$
3. Mirroring the constraint over the (Y, Z)-plane: $\psi = -\psi_{\mathbb{R}^3_+} + \pi$.

Note that $\psi \in [0, 2\pi)$, which can be enforced by taking the 2π modulus of ψ. In the remainder of this paper constraints are assumed to lie in $\mathbb{R}^3_+$, unless specifically mentioned. The domain of the constraint angles changes to

$$\begin{array}{l} \gamma_c \in [0, \pi/2] \\ \chi_c \in [0, \pi/2]. \end{array} \qquad (13)$$

Resulting ψ for constraints in any other direction can be derived from the results for the positive orthant.

2.3. Relative Orbit Design Problem Formulation

The design of relative orbits in the presence of geometric constraints can be formulated as an optimization problem. If the goal is to design a relative orbit that minimizes the risk of violating the geometric constraint, this optimization problem can be formulated as:

$$\text{max.} \quad \alpha_{\min}\left(\psi\right) \quad \text{for} \quad \psi \in [0, 2\pi) \qquad (14)$$
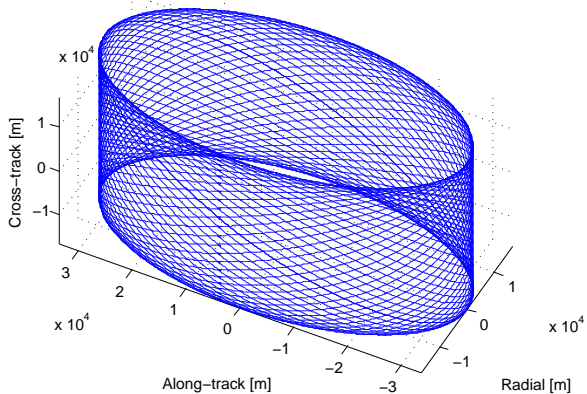
4

Figure 6: Elliptical cylinder from relative motion orbits, formed by tracing out ψ from 0 to 2π in 50 steps.

Constraints can be added to the problem, such as

- $\alpha_{\min} > \beta/2$: respecting the sensor's field of view
- $\psi < 30\,\mathrm{deg}$: limits on ψ, e.g. if e/i-vector separation strategy is used
- limits on $a\|\Delta\mathbf{e}\|$ and $a\|\Delta\mathbf{i}\|$

Alternatively, the optimization problem could also be reformulated to a feasibility problem, e.g., find ψ subject to the contraints. However, by maximizing $\alpha_{\min}$, a margin is created, which, in the presence of uncertainty, can be helpful to ensure satisfaction of the constraints.

3. Results

One of the key results that can be obtained from the presented theory can be visualized in two figures that show the maximum achieveable $\alpha_{\min}$ and the corresponding relative phase angle ψ for a constraint pointing in an arbitrary direction in $\mathbb{R}^3_+$. These figures have been generated for the cases $a\delta e = a\delta i$. In order to construct these graphs, a grid was defined in terms of γ_c and χ_c, over the positive orthant. For each node on the grid, $\alpha_{\min}$ was derived for all relative phase angles ψ between 0 and 2π. The largest $\alpha_{\min}$ and the corresponding ψ were plotted respectively in Figures 7 and 8.

Figure 7 is a combination of a surface and a contour plot that shows the maximum $\alpha_{\min}$ over all values of ψ for a constraint pointing in any direction in $\mathbb{R}^3_+$. Figure 8 shows at which angle ψ the maximum $\alpha_{\min}$ is achieved. If the constraint direction is known in terms of angles γ_c and χ_c, the largest
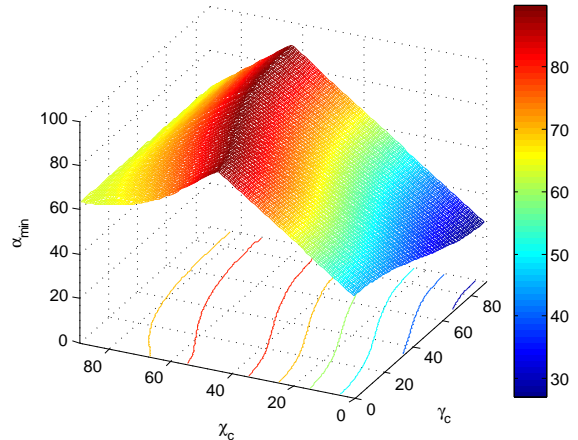

Figure 7: Maximum $\alpha_{\min}$ over all ψ for a constraint in $\mathbb{R}^3_+$, defined by γ_c and χ_c.

achieveble $\alpha_{\min}$ can be read from Figure 7. Figure 8 will give the corresponding angle ψ at which this $\alpha_{\min}$ is achieved. This can be used as a first guess for the relative phasing angle ψ in the design of a relative orbit. In an early design stage it could also be used to, e.g., place a star sensor on a satellite as constraints in certain directions are easier to cope with than constraints in other directions. The plot shows for example that constraints in the (X,Y)-plane are generally more difficult to deal with, while constraints with an elevation χ_c between $30°$ and $60°$ guarantee an $\alpha_{\min}$ larger than $60°$.

Figures 7 and 8 were generated in two ways:

1. By determining $\mathbf{e}_\perp$ from Eqs. 10-12 and calculating $\alpha_{\min}$ from Eq. 7.
2. By propagating the relative motion and evaluating α at every point in the relative motion orbit to obtain $\alpha_{\min}$.

Evidently, the second method was far more computationally demanding (i.e., many hours for a 50x50 grid, vs. seconds for the first method on a 2.9 GHz processor). The second method served also to validate the expressions presented in Equations 7-12.

3.1. Orbit Design Process

The sequence of activities for designing relative orbits in the presence of geometric constraints can be summarized as follows:

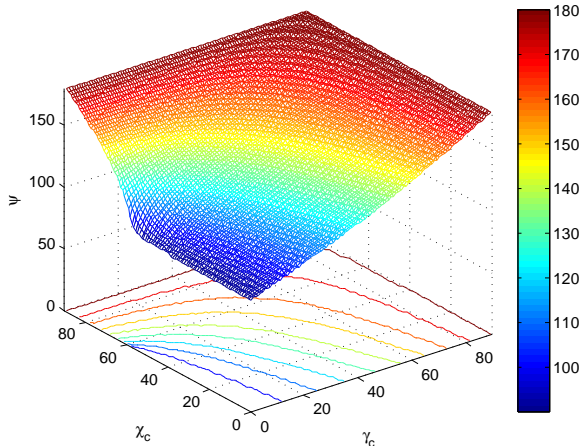1. Identify the geometric constraint(s) and express the constraints in terms of γ_c, χ_c and $\beta/2$.

Figure 8: Relative phase ψ corresponding to the maximum $\alpha_{\min}$ in Figure 7.

2. Identify other constraints (e.g., a limited domain of ψ that guarantees separated eccentricity and inclination vectors).
3. Identify the domain of $a\delta e$ and $a\delta i$.
4. Formulate the problem (e.g., find the ψ that maximizes $\alpha_{\min}$).
5. Solve the problem (i.e., find ψ).
6. Specify eccentricity and inclination vectors that have relative phasing angle ψ.

The application of this process is demonstrated in the next subsection.

3.2. Exemplary Case

The following example serves to demonstrate how the theory developed in this paper can be applied to design relative orbits in the presence of geometric constraints. This sample case consist of four collocated satellites in GEO, where one of the satellites (or each, there is no difference) is equipped with a nadir-pointing sensor and a north-looking star sensor. In addition, separated eccentricity and inclination vectors are desired to prevent the radial and out-of-plane separations to vanish simultaneously. This last constraint translates into boundaries on the relative phasing angle ψ. The constraints are specified in Table 1. Note that the star sensor is not exactly facing north, as this side is usually equipped with solar panels that would otherwise obstruct the field of view.

The reference orbit is a perfect circular geostationary orbit with zero inclination. Its state vector,

Table 1: Definition of constraints for sample case

Constraint 1: nadir-pointing sensor
$\gamma_{c1} = 0°$, $\chi_{c1} = 0°$, $\beta_1/2 = 9°$

Constraint 2: north-looking star sensor
$\gamma_{c2} = 45°$, $\chi_{c2} = 75°$, $\beta_2/2 = 15°$

Contraint 3: Bounds on ψ for e/i separation
$\psi \in [0°, 30°] \cup [150°, 210°] \cup [330°, 360°]$

according to the convention in Equation 1, is:

$$\mathbf{E}_{\text{ref}} = (a_{\text{ref}}, 0, 0, 0, 0, 0)^T, \qquad (15)$$

where $a_{\text{ref}} = 42{,}164$ km is the geostatiory orbit radius. This analysis considers only pure Keplerian two-body dynamics, thus no specific epoch is assumed. The goal in this example is to define the relative orbital elements with respect to $\mathbf{E}_{\text{ref}}$, using the parameterization as given by Eq. 2. Relative eccentricity and inclination are assumed to be equal, i.e. $\delta e = \delta i$, for each individual satellite.

Following the structure provided in Section 2, the relative orbit design problem can be formulated as follows:

maximize $\quad \min(\alpha_{\min 1}(\psi), \alpha_{\min 2}(\psi))$

subject to:

$\psi \in [0°, 30°] \cup [150°, 210°] \cup [330°, 360°]$.
$\alpha_{\min 1} > \beta_1/2$
$\alpha_{\min 2} > \beta_2/2$
$\delta e = \delta i$

In this problem definition, $\alpha_{\min 1}$ and $\alpha_{\min 2}$ are the minimum angles as defined by Figure 4 for constraint #1 and #2, respectively. This problem can be solved numerically by defining a grid of possible values of ψ and evaluating $\alpha_{\min 1}$ and $\alpha_{\min 2}$ at each point in the grid. However, the problem is further analysed here in order to obtain additional insight. The effect of constraint #3 on the achieveable $\alpha_{\min}$ is investigated. Two contour plots equivalent to Figures 7 and 8 are generated, but now including the constraints on ψ. The resulting plots are given in Figures 9 and 10. The locations of the constraints are indicated by black dots (note that constraint #1 is shown in the bottom left corner). From Figure 9, some important observations can be made:
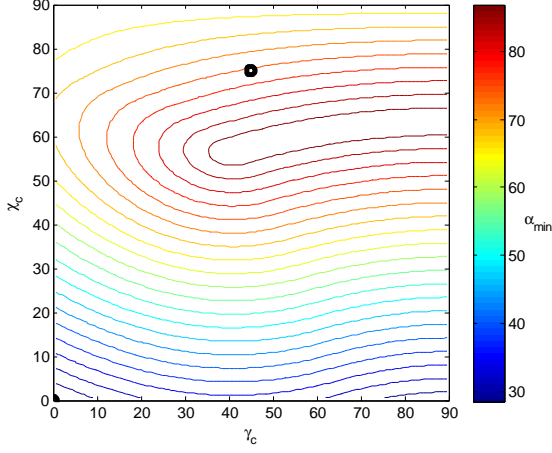
6

Figure 9: Maximum $\alpha_{\min}$ for constrained ψ. Black dots are the example case constraints.

Figure 10: Relative phase ψ corresponding to the maximum $\alpha_{\min}$ in Figure 9.

- Both constraints can be dealt with individually as $\alpha_{\min}$ is larger than $25°$.
- The nadir-pointing constraint (constraint 1) seems more challenging to satisfy as the margin for $\alpha_{\min}$ is much smaller in the feasible region.

If these graphs would already indicate an infeasible constraint, a relaxation of constraints would be necessary.

The next step is to find out if both constraints can be dealt with simultaneously. To that end, a plot is made that shows how $\alpha_{\min}$ varies if the relative phase angle is varied between 0 and 2π. The result is shown by the thick green and blue lines in Figure 11.

The first observation from this figure is that constraint 2 is passively dealt with for any choice of ψ. The constraint on ψ is shown by the red boxes. Constraint 1 is indicated by green shaded area. As per our expectation from Figures 9 and 10, all three constraints can be dealt with. The acceptable values for ψ are as follows:

$$\psi \in [10, 30] \cup [150, 170] \cup [190, 210] \cup [270, 290]. \quad (16)$$

As stated in the introduction, knowledge on the along-track position is generally poor, which renders it difficult to accurately control the along-track position. Expressed in relative orbital elements, this results in variations in $\Delta\lambda$. The impact of these variations has been investigated for this example case. The dashed lines in Figure 11 show how $\alpha_{\min}$ changes if $\Delta\lambda$ is varied between -10^{-4}
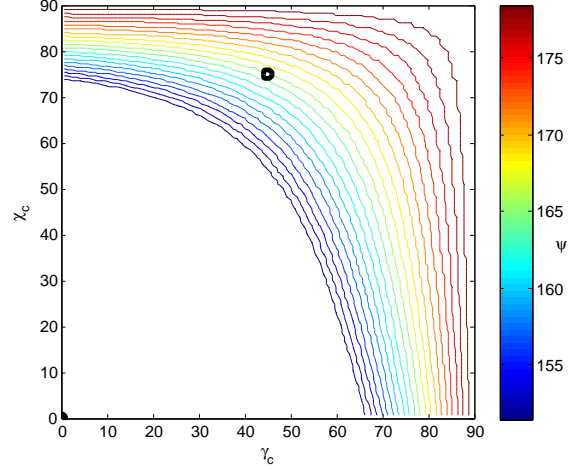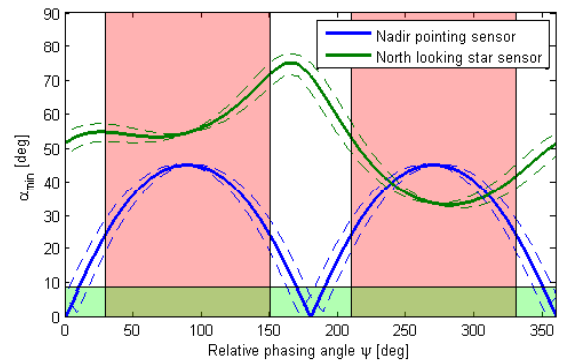

Figure 11: Variation of $\alpha_{\min}$ for ψ between 0 and 2π

Figure 12: Placement of eccentricity and inclination vectors for sample case 1
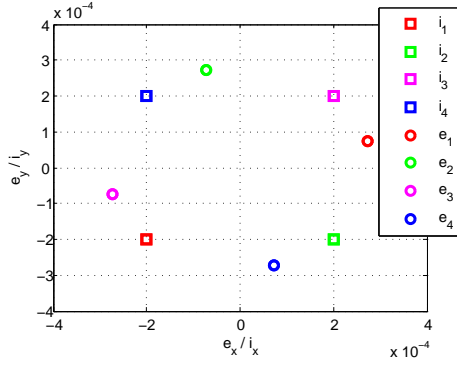

Figure 13: Placement of eccentricity and inclination vectors for sample case 2

and 10^{-4} rad. Looking at the Nadir pointing sensor, a near horizontal shift is observed. This results in a smaller set of acceptable angles ψ. Finally, Figure 11 is used to select the desired ψ from the set of acceptable values in Eq. 16. In this example, $\psi = 150°$ is taken, since it results in the largest margin for the star sensor, amongst the (four) points that maximize the margin for the Nadir pointing sensor.

The choice of ψ restricts the relative orientation of eccentricity and inclination vectors. However, it leaves us completely free to place either inclination or eccentricity vectors (the other being constrained to a line by ψ and to an arc through $\delta e = \delta i$, the intersection of which is a point). As an example, two inclination vector configurations have been specified in Table 2. The corresponding eccentricity vectors are completely defined through ψ and $\delta e = \delta i$. The endpoints of these vectors are marked in Figures 12 and 13.

Table 2: Specification of two configurations of inclination vectors. All values in $\cdot 10^{-4}$ rad.

	Case 1		Case 2	
	i_x	i_y	i_x	i_y
Sat1	−2.0	−2.0	0	−2.5
Sat2	2.0	−2.0	0	−0.5
Sat3	2.0	2.0	0	1.5
Sat4	−2.0	2.0	0	3.5

The relative orbital elements according to Eq. 2 are now completely specified for all four satellites (note that $\Delta E_1 = \Delta E_2 = 0$ was implicitly assumed). The resulting relative orbits have been simulated for both cases. Figures 14 and 15 show
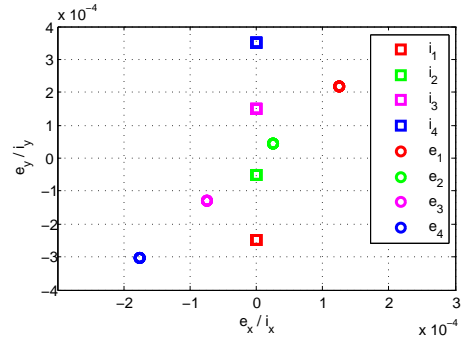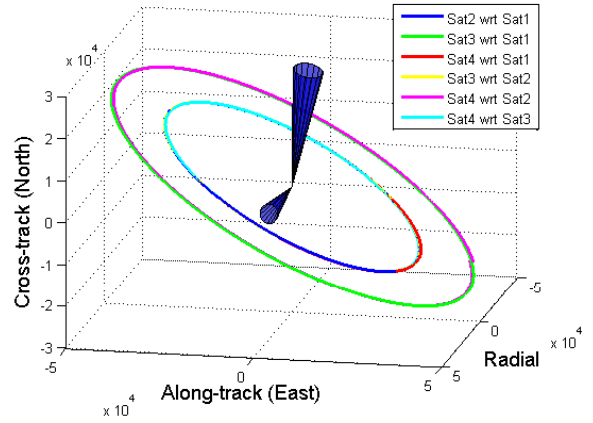

Figure 14: Relative orbits in the presence of geometric constraints for each satellite pair, case 1

the relative orbits of a satellite about another satellite for each pair of satellites. The other satellite is in the center of the coordinate system, equipped with both sensors. The fields of view are indicated by the cones. All satellites can be equipped with an identical set of sensors without violation of the constraints.

Figure 16 shows the relative orbits for case 2 in the Hill frame of the reference (specified by the orbital elements in Eq. 15). As the size δi is different for each satellite, the size of the relative orbit is different. A similar graph for case 1 would show all four satellites being in the exact same relative orbit with respect to the reference orbit.

Figure 17 shows the effect of variations in $\Delta \lambda$ between $-2 \cdot 10^{-4}$ and $2 \cdot 10^{-4}$ rad, for the relative motion of sat2 about sat1. The constraints are still respected, but for the nadir-pointing sensor, this is close to the allowable tolerance.
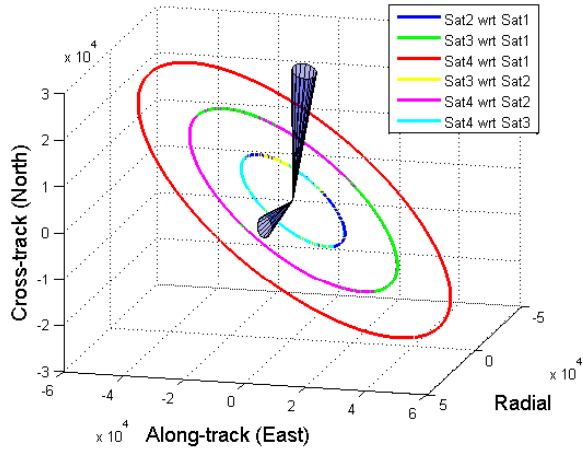
Figure 15: Relative orbits in the presence of geometric constraints for each satellite pair, case 2
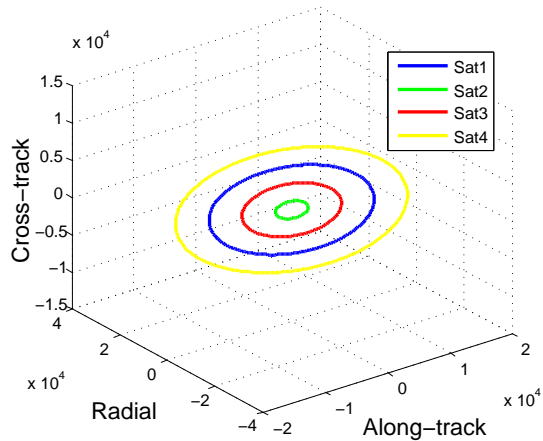

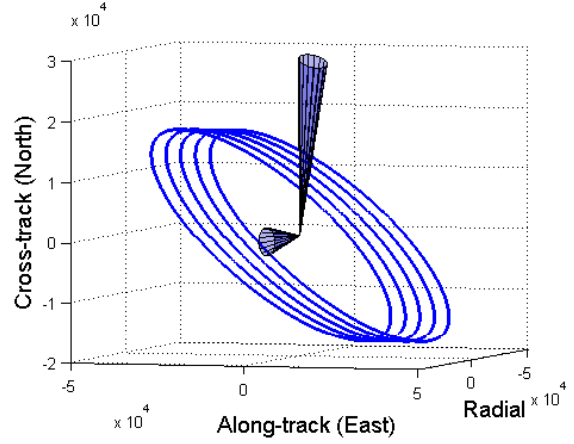Figure 16: Relative orbits about the reference orbit, case 2

Figure 17: Effect of variations in $\Delta\lambda$ on the relative orbit of sat1 around sat2, case 1

4. Discussion

The theory and results presented in this paper allow to support design of relative orbits in the presence of geometric constraints. However, to arrive at these results, some simplifying assumptions have been made, which should be accounted for when applying the theory.

4.1. Domain of Validity

The analysis in this paper focused on an application to collocated satellites in a geostationary orbit. The orbits were assumed to be near-circular and the sensors were assumed to be non-rotating in the Hill frame (e.g., nadir-pointing). The validity of the results for eccentric orbits needs to be be further analyzed. For rotating sensors, the results can not be extended, unless the rotation is constrained to a cone with a fixed orientation in the Hill frame. The sensors on the different satellites in the cluster are assumed to be pointing in identical directions. The developed guidelines can be applied as well to support a heuristic relative orbit design for clusters with non-homogeneous sensor directions. However, the analysis quickly becomes complicated for clusters with a multitude of sensors pointing in arbitrary directions.

The paper focused on formations around the same mean argument of longitude. Thus trailing formations or pendulum type formations, where such geometric constraints may be trivial, are excluded from the analysis. For non-zero variations in $\Delta\lambda$ the geometric relations, derived in Section 2, loose their

validity. However, for small variations in $\Delta\lambda$ they are still good approximations.

4.2. Real-World Considerations

The current study assumes perturbation-free dynamics, where the satellites are assumed to be perfectly controlled on pure Keplerian orbits. In reality, perturbations disturb the ideal relative orbits and control is required to prevent this. To deal with most sensor constraints, it will be required to actively control the relative mean argument of longitude, so that the relative motion orbits remain centered. This can be a challenge to deal with, as also orbit determination errors in along-track direction are typically dominating, and geostationary satellites generally have only weekly maneuvers with long drift periods. Especially when also maneuver execution errors and thruster cross couplings are considered [7], the task of controlling relative motion in the presence of these new constraints can be tedious. However, with the availability of onboard orbit determination capability through, e.g., GPS receivers and more frequent control action with, e.g., electric propulsion, these challenges could be addressed in the near future.

5. Conclusion and Outlook

The paper introduced a method to include geometric constraints in terms of a sensor's pointing direction and field of view in the design of relative motion of orbits of collocated satellites. The underlying geometry has been analysed for relative orbits in near-circular orbits centered on the same mean argument of longitude. From this geometric analysis, key relations were established between relative orbital elements and the geometric constraints. These relations can be used in the design of relative orbits or support the placement of sensors onboard collocated satellites. To that end a design process was developed. An example demonstrated the application of this process to the design of relative orbits for collocated satellites in a geostationary orbit, in the presence of nadir-pointing sensors and north-looking star sensors.

The domain of validity of this research is limited to ideal conditions such as pure Keplerian motion and further analysis needs to be done to extent the results to other orbits, e.g. eccentric orbits. Furthermore, the impact of orbit determination and control accuracy in the presence of

perturbing forces will play a crucial role in the possibility to maintain relative orbits that respect the geometric constraints. These challenges will be addressed in future work.

6. References

[1] M. Eckstein, C. Rajasingh, P. Blumer, Colocation strategy and collision avoidance for the geostationary satellites at 19 degrees west, in: International Symposium on Space Flight Dynamics, 1989.

[2] O. Montenbruck, R. Kahle, S. D'Amico, J. Ardaens, Navigation and control of the tandem-x formation, Journal of the Astronautical Sciences 56 (3) (2008) 341.

[3] S. D'Amico, Autonomous Formation Flying in Low Earth Orbit, Ph.D. thesis, Delft University of Technology (2010).

[4] J. Wang, S. Nakasuka, Cluster flight orbit design method for fractionated spacecraft, Aircraft Engineering and Aerospace Technology 84 (5) (2012) 7–7.

[5] P. Wauthier, P. Francken, The astra co-location strategy for three to six satellites, Revista Brasileira de Ciencias Mecanicas (ISSN 0100-7386), vol. 16, p. 163-171 16 (1994) 163–171.

[6] H. Schaub, K. Alfriend, J 2 invariant relative orbits for spacecraft formations, Celestial Mechanics and Dynamical Astronomy 79 (2) (2001) 77–95.

[7] M. Eckstein, Geostationary orbit control considering deterministic cross coupling effects, in: Dresden International Astronautical Federation Congress, Vol. 1, 1990.